Review

Recent Advances of Fluorescence Probes for Imaging of Ferroptosis Process

Hongyu Li [1,2,3], Yan An [1,2,3], Jie Gao [1,2,3], Mingyan Yang [1,2,3], Junjun Luo [1,2,3], Xinmin Li [1,2,3], Jiajia Lv [1,2,3], Xiaohua Li [4,*], Zeli Yuan [1,2,3,*] and Huimin Ma [4]

1   College of Pharmacy, Zunyi Medical University, Zunyi 563003, China; lihongyu@iccas.ac.cn (H.L.); anyan9698@126.com (Y.A.); jiegao@mail.nankai.edu.cn (J.G.); myyoung@whut.edu.cn (M.Y.); luojunjun8868@163.com (J.L.); lixinmin19@126.com (X.L.); lvjiajia1218@foxmail.com (J.L.)
2   Key Laboratory of Basic Pharmacology of Ministry of Education and Joint International Research Laboratory of Ethnomedicine of Ministry of Education, Zunyi Medical University, Zunyi 563000, China
3   Guizhou International Scientific and Technological Cooperation Base for Medical Photo−Theranostics Technology and Innovative Drug Development, Zunyi 563003, China
4   Key Laboratory of Analytical Chemistry for Living Biosystems, Institute of Chemistry, Chinese Academy of Sciences, Beijing 100190, China; mahm@iccas.ac.cn
*   Correspondence: lixh@iccas.ac.cn (X.L.); zlyuan@zmu.edu.cn (Z.Y.)

Abstract: Ferroptosis is an iron−dependent form of regulated cell death. It has attracted more and more research interests since it was found because of its potential physiological and pathological roles. In recent years, many efforts have been made for the developments and applications of selective fluorescence probes for real−time and in situ tracking of bioactive species during ferroptosis process, which is necessary and significant to further study the modulation mechanisms and pathological functions of ferroptosis. In this review, we will focus on summarizing the newly developed fluorescence probes that have been applied for ferroptosis imaging in the recent years, and comprehensively discussing their design strategies, including the probes for iron, reactive oxygen species, biothiols and intracellular microenvironmental factors.

Keywords: ferroptosis; fluorescence probe; iron; reactive oxygen species; biothiols; intracellular microenvironment

1. Introduction

Ferroptosis is a newly found form of regulated cell death by Stockwell and co−workers in 2012 [1], which is highly dependent on the participation of intracellular iron. More and more research has shown that ferroptosis is closely related with many critical diseases, such as neurodegeneration, cancer, ischaemic organ injuries and autoimmune diseases [2–5]. Meanwhile, the modulation of cancer cell ferroptosis also provides new strategy to precision antitumor drug design [6–10]. Ferroptosis is executed by the accumulation of lipid peroxides to lethal levels. In ferroptosis, the lipid peroxidation of polyunsaturated fatty acids can be induced by two different pathways [11,12]: one is blocking cystine uptake of the cystine/glutamate antiporter system x_c^- on cell membrane by ferroptosis inducer such as erastin, to deplete intracellular biothiols, including cysteine (Cys) and its downstream product glutathione (GSH), and finally cause the inactivation of the main lipid peroxides eliminator glutathione peroxidase 4 (GPX4) [1,13,14]; the other one is the covalent inactivation of GPX4 by some specific GPX4 inhibitors (e.g., RSL3) [15]. It is clear that iron, reactive oxygen species (ROS) and biothiols play crucial and highly related roles in the development and redox regulation in ferroptosis (Figure 1). Therefore, efficient detection methods that enable the real−time and in situ tracking of these bioactive species are necessary and significant to further study the modulation mechanisms and pathological functions of ferroptosis.
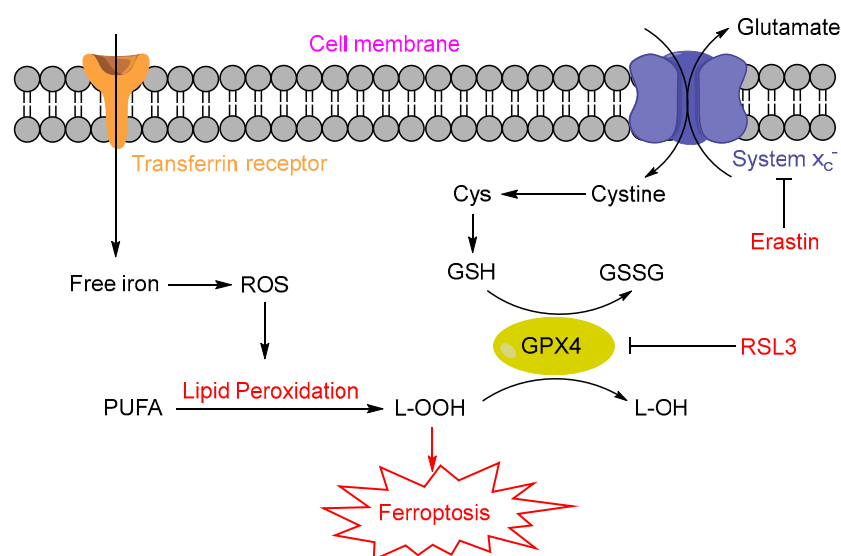
Figure 1. A brief illustration for the roles of iron, reactive oxygen species and biothiols in the development and redox regulation in ferroptosis. Abbreviations: Cys, cysteine; GSH, reduced glutathione; GSSG, oxidized glutathione; GPX4, glutathione peroxidase 4; ROS, reactive oxygen species; PUFA, polyunsaturated fatty acid; L−OOH, lipid peroxides; L−OH, lipid alcohols.

Fluorescence probes have long been used for bioimaging due to their sensitive, high−resolution and noninvasive properties [16–18], for example, imaging of ROS [19–21], biothiols [22–24] and cell microenvironmental factors (e.g., viscosity and polarity) [25]. Commercially available probes, for instance, ROS responsive probe $2',7'$−dichlorodihydrofluorescein diacetate (H_2DCFDA) and lipid peroxides responsive C11−BODIPY$^{581/591}$ are capable of the visualized analysis for ferroptosis [1,26,27]. However, these probes can only monitor the total amount of ROS or lipid peroxides, lack selectivity for a certain bioactive species. Thus, in recent years, many efforts have been made for the developments and applications of selective fluorescence probes for ferroptosis. In this review, we will focus on summarizing the newly developed fluorescence probes that have been applied for ferroptosis imaging in the recent years, and comprehensively discussing their design strategies, including the probes for iron, reactive oxygen species, biothiols and intracellular microenvironmental factors.

2. Fluorescence Probes for Iron and Its Related Bioactive Species

As one of the central regulators for ferroptosis process, iron is indispensable for the accumulation of lipid peroxides. The import, export and storage of iron greatly impact the cell sensitivity for ferroptosis [11]. On one hand, the iron−participated Fenton reaction and Haber–Weiss reaction directly contribute to the cell ROS pool [28,29], including hydroxyl radical (•OH), superoxide ($O_2^{•-}$), hydroperoxyl radical (•OOH) and hydrogen peroxide (H_2O_2), which are the main initiators for lipid peroxidation process [30,31]. On the other hand, some iron−containing enzymes, such as lipoxygenase, are also essential promotors of lipid peroxidation [32]. Thus, the detection of intracellular iron during ferroptosis, especially distinguishing iron of different valence states, is significant for ferroptosis studies.

2.1. Probes for Fe^{2+} and Heme

Despite its importance for many life processes, fluorescence probes for selective detection of labile ferrous ion (Fe^{2+}) within living cells remain limited. A main reason is the fluorescence quenching property of Fe^{2+} ion, due to its unpaired electrons on d−orbit. Fe^{2+} would act as a fluorescence quencher by electron and/or energy transfer after chelating with a fluorescence probe. Therefore, chelation−based Fe^{2+} probes often present fluorescence turn−off response, which is undesirable for their applications in biological systems [33,34].

In addition, the binding ability of Fe^{2+} is relatively weaker comparing to other metal ions [35], which may cause poor selectivity for Fe^{2+}.

To address these problems, Chang's group [36] sought to design a reactivity−based probe design strategy by which Fe^{2+} selectively reacts with a caged probe to release the fluorophore rather than binding. The developed probe FIP−1 is inspired by the antimalarial agents such as artemisinin that contains a Fe^{2+}−cleavage endoperoxide moiety, as shown in Figure 2A. Based on fluorescence resonance energy transfer (FRET), FIP−1 was designed by connecting a 5−aminomethyl fluorescein (5−AMF, FRET donor) and a cyanine 3 (Cy3, FRET acceptor) by an Fe^{2+}−cleavable endoperoxide linker. FIP−1 itself showed two absorption peak at 495 and 545 nm, which is assigned to 5−AMF and Cy3, respectively. Meanwhile, due to the FRET effect, it fluoresced at 515 and 556 nm. When exposed to Fe^{2+}, the cleavage of endoperoxide linker could block the FRET effect from 5−AMF to Cy3, resulting in obvious fluorescence increase at 515 nm. FIP−1 showed no response to other common metal ions, such as Fe^{3+}, Cu^{2+}, Mg^{2+}, K^+, Ca^{2+}, Mn^{2+}. However, Cu^+ at 10 μM level could induce non−negligible fluorescence response. FIP−1 was then applied to detect the changes in labile iron pools (i.e., free Fe^{2+} and Fe^{2+} weakly bound to cellular ligands) during ferroptosis initiated by a newly reported ferroptosis inducer 35MEW28. As seen in image b of Figure 2B, MD−AMB−231 cells treated with ferroptosis inducer 35MEW28 exhibited obviously increased level of the labile iron pool. The co−incubation of cells with 35MEW28 and deferoxamine (DFO, a Fe^{2+} scavenger) did not result in a change in labile iron pools compared to control group. However, the co−treatment with 35MEW28 and the lipophilic antioxidant Fer−1 does not alter the labile iron pools compared to cells treated with 35MEW28 alone. These results suggest that cell ferroptosis process exhibited increased labile Fe^{2+} levels.
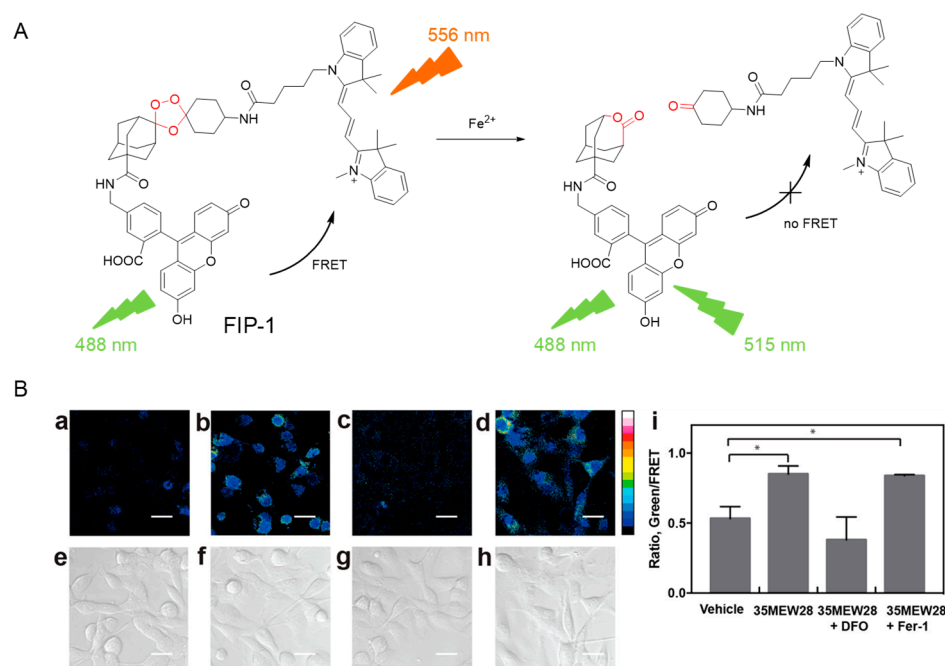

Figure 2. The FRET−based Fe^{2+} probe FIP−1 and its application in imaging of changes in labile iron pools during 35MEW28−initiated ferroptosis of MD−AMB−231 cells. (**A**) Response mechanism of FIP−1 to Fe^{2+}. (**B**) Fluorescence imaging of FIP−1 in MDAMB−231 cells treated with (**a**) vehicle, (**b**) 35MEW28, (**c**) 35MEW28 + DFO, and (**d**) 35MEW28 + Fer−1. (**e–h**) Bright field images of (**a–d**). (**i**) Mean Green/FRET ratios of MDA−MB−231 cells. Statistical significance was assessed by calculating p−values using one−way ANOVA with the Bonferroni correction in R, * $p < 0.05$. Reprinted/adapted with permission from Ref. [36]. Copyright 2016, American Chemical Society.

Another reactivity−based approach for Fe^{2+} selective probe is the Fe^{2+}−triggered deoxygenation of dialkylarylamine N−oxide. As depicted in Figure 3, fluorophore with a dialkylarylamine N−oxide group is usually non−fluorescent as the photoinduced electron transfer (PET, a non−radiative process) from the N−oxide group to fluorophore. However, the selective deoxygenation of dialkylarylamine N−oxide moiety by Fe^{2+} can recover the fluorescence of the connected fluorophore, which offers a universal design method for functionalized Fe^{2+} probe by modifying varied fluorophore with dialkylarylamine N−oxide group [37,38]. Based on this approach, Hirayama et al., reported a series of organelle−targetable Fe^{2+} probe MtFluNox (mitochondria targeting) [39], Lyso−RhoNox (lysosome targeting) [40], and ER−SiRhoNox (endoplasmic reticulum targeting) [41], and applied them to monitor organelle Fe^{2+} level change in ferroptosis [42]. Through the selective deoxygenation reaction with Fe^{2+}, these probes presented significant fluorescence turn−on at 535 nm (MtFluNox), 575 nm (Lyso−RhoNox) and 660 nm (ER−SiRhoNox) with similar reaction rates. The reaction rate constants of MtFluNox, Lyso−RhoNox, and ER−SiRhoNox with Fe^{2+} were tested to $2.1 \times 10^{-3} s^{-1}$, $2.2 \times 10^{-3} s^{-1}$, and $1.7 \times 10^{-3} s^{-1}$, respectively. In addition, colocalization imaging showed high Pearson's correlation value of these probes with the corresponding commercial organelle−targetable dyes, for instance, 0.81 ± 0.03 for Ac−MtFluNox (acetylated form of MtFluNox, more cell−compatible) with MitoTracker DeepRed, 0.80 ± 0.02 for Lyso−RhoNox with LysoTracker Green DND−26, and 0.80 ± 0.02 for ER−SiRhoNox with ER−Tracker Green, implying their good organelle−targeting ability. These properties enable the simultaneous multi−color imaging of labile Fe^{2+} levels at each targeted organelle. With the fluorescence imaging of these probes, the authors found that ferroptosis of HT−1080 cells induced by erastin showed aberrant elevation of labile Fe^{2+} in the lysosomes and endoplasmic reticulum.
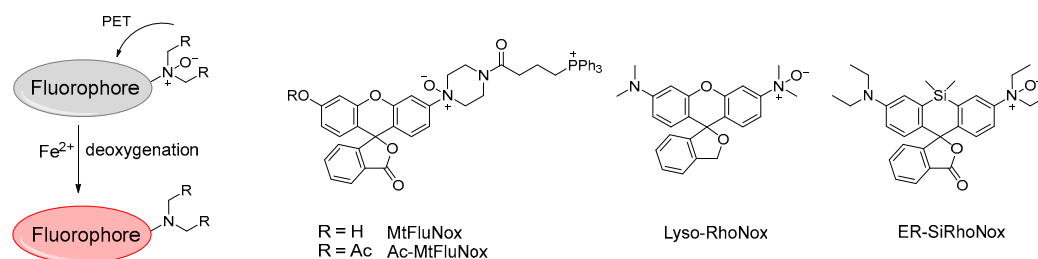

Figure 3. Structures of organelle−targetable Fe^{2+} probe MtFluNox, Lyso−RhoNox, ER−SiRhoNox and their general response mechanism to Fe^{2+} [42].

Interestingly, based on the above−mentioned N−oxide deoxygenation strategy, Hirayama et al. [43] further reported a selective fluorescence probe H−FluNox for intracellular labile heme (i.e., complex of Fe^{2+} and protoporphyrin IX, an essential protein cofactor), as well as its applications in ferroptosis process. The design of H−FluNox was inspired by the biomimetic reaction of cytochrome P450 with tetramesitylporphyrin iron complex and perbenzoic acid derivatives (Figure 4A) [44], in which the cleavage of O−O bond was accelerated by the electron−withdrawing aryl group. Therefore, an electron−withdrawing 4,4−difluoropiperidine N−oxide recognition group was introduced to facilitate the deoxygenation reaction of N−oxide group by labile heme (Figure 4B). At the same time, the relative slow reaction rate of the probe toward labile Fe^{2+} could limit the response to Fe^{2+} and enable a selective response to labile heme. When hemin (1 μM) was added to H−FluNox (0.2 μM) in the presence of 100 μM GSH, a rapid fluorescence increase at 535 nm was observed and reached 230−fold within 10 min. By contrast, the addition of Fe^{2+} (10 μM) resulted in only a less 10−fold fluorescence increase even after incubation for 30 min. Besides, Fe^{3+} and hemin (in the absence of GSH) would not affect the detection of Fe^{3+}. The high selectivity of H−FluNox to labile heme enables the discrimination of labile heme from other intracellular iron related bioactive species in living cells. Fluorescence imaging with the Ac−H−FluNox (acetylated form of H−FluNox, more cell−compatible) could monitor the changes in the intracellular labile heme levels with the exogenous acti-

vation or inhibition, such as nitric oxide−induced labile heme release and accumulation of heme by inhibition of its exporter. Finally, imaging with Ac−H−FluNox demonstrated that the labile heme level was upregulated upon the induction of ferroptosis by erastin in HT−1080 cells.
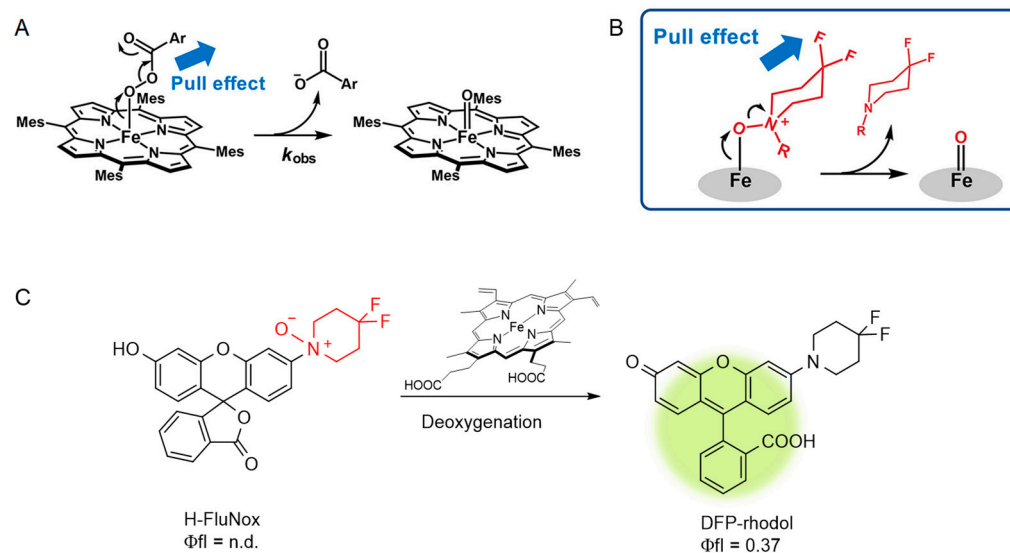

Figure 4. (**A**) Biomimetic reaction of cytochrome P450 with tetramesitylporphyrin iron complex and perbenzoic acid derivatives. (**B**) Design strategy of heme−selective probe. (**C**) Structure of H−FluNox and its fluorescence turn−on response mechanism with Fe^{2+}. Reprinted/adapted with permission from Ref. [43]. Copyright 2022, American Chemical Society.

Similarly, Xing et al. [45] reported another selective reaction−based probe COU−LIP−1 by the Fe^{2+}−triggered N−O bond cleavage and applied it for monitoring intracellular labile Fe^{2+} pools (Figure 5). COU−LIP−1 was designed by utilizing coumarin 343 as the fluorophore and 3−nitrophenylazanyl ester as both the recognition group and the fluorescence quenching group. In the absence of Fe^{2+}, as the PET process from coumarin 343 to 3−nitrophenylazanyl ester group, the fluorescence of COU−LIP−1 was efficiently quenched. However, after COU−LIP−1 reacting with Fe^{2+}, the Fe^{2+}−induced reductive cleavage of the N–O bond could release the fluorescent coumarin 343 fluorophore, resulting in a significant fluorescence intensity increase at 488 nm. Selectivity studies showed that COU−LIP−1 is selective for Fe^{2+} over various metal ions (such as Mn^{2+}, Fe^{3+}, Cu^{2+}, Co^{2+}, Cu^+), ROS (such as •OH, H_2O_2, OCl^-) and reductive species (such as Na_2S, ascorbic acid, Cys, GSH). COU−LIP−1 was then applied for the study of labile Fe^{2+} level changes in erastin−induced ferroptosis via confocal fluorescence imaging and cytometry analysis. The results showed a time−dependent fluorescence intensity increase in HT−1080 cells treated with erastin to induce ferroptosis, suggesting the increase in labile Fe^{2+} level. COU−LIP−1 was also employed for monitoring labile Fe^{2+} level changes in different activated states of the RAW 264.7 macrophages. Significant higher labile Fe^{2+} level was observed in M1 macrophages (activated by lipopolysaccharides) than M0 macrophages (untreated RAW 264.7 cells) and M2 macrophages (activated with IL−4). Interestingly, when subjected to erastin−induced ferroptosis, M0 and M1 macrophages displayed opposite labile Fe^{2+} level changes. Labile Fe^{2+} level showed time−dependent increases in M0 macrophages but decrease in M1 macrophages upon the erastin treatment.
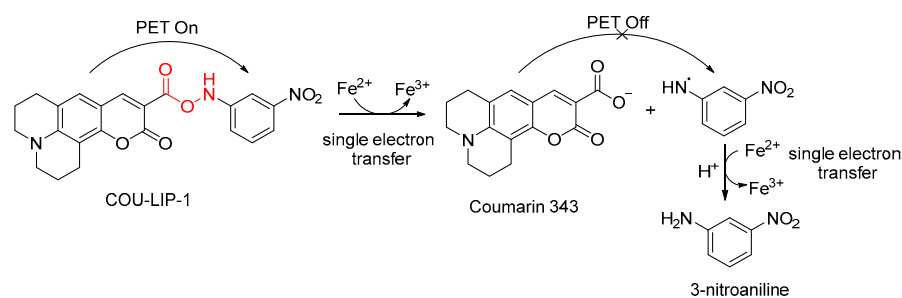
Figure 5. The fluorescence turn−on response mechanism of COU−LIP−1 to Fe^{2+} [45].

2.2. Probes for Fe^{3+}

In general, there are three basic response modes for fluorescence probe [17]: turn−off response, that is, fluorescence of the probe gets quenched in response to the analytes; by contrast, turn−on response, namely, fluorescence of the probe increases in the presence of analytes, which provides a higher signal−to−noise ratio than the turn−off response. Compared to the above two response modes, which involve monitoring fluorescence intensity change at one wavelength, ratiometric response, which involves detecting the ratio of fluorescence intensities at two wavelengths, has many advantages, such as eliminating the interferences from sample matrix, excitation source laser intensity fluctuation, microenvironment around probes, and concentration errors of probes [17,46]. Therefore, a ratiometric probe is more suitable for an accurate quantitative analysis.

In 2019, Lin's group [47] developed a ratiometric Fe^{3+} probe P1 by connecting two rhodamine Schiff base and a polysiloxane moiety by imine−linker (Figure 6). The polysiloxane moiety of P1 showed blue emission at 490 nm, which could be quenched in the presence of Fe^{3+}. However, in response to Fe^{3+}, the rhodamine lactam moiety could get ring−opening to produce fluorescence increase at 589 nm, which favors the ratiometric detection of Fe^{3+} with fluorescence intensity ratio change. P1 is selective for Fe^{3+} over other metal ions, including Fe^{2+}, Co^{2+}, Cu^{2+}. On the other hand, this polymer probe is difficult to permeate the cell membrane, due to its large molecular weight. Thus, P1 could only stain dead cells (e.g., apoptotic cells and ferroptotic cells) because of the destructive membrane, while live ones did not show any fluorescence. Therefore, in the apoptotic cells, P1 presented its inherent blue fluorescence, whereas in the case of ferroptosis, as the level of Fe^{3+} increased, P1 presented red fluorescence of rhodamine. Thus, P1 could be used as an effective chemical tool for selectively targeting apoptosis cancer cells and real−time imaging of ferroptosis process.
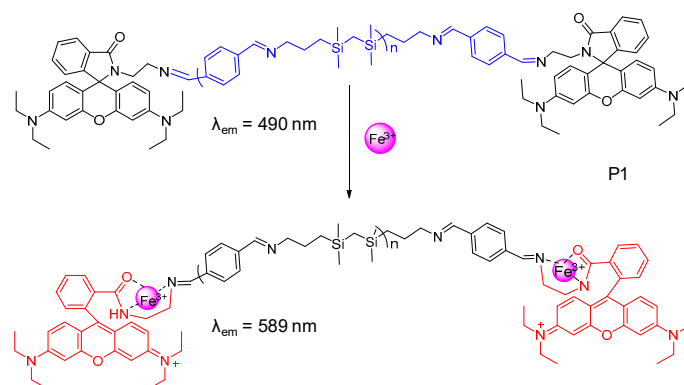

Figure 6. The ratiometric response mechanism of P1 to Fe^{3+} [47].

Another ratiometric Fe^{3+} probe DRhFe was developed and applied in tracking of endogenous Fe^{3+} in ferroptosis by He's group (Figure 7) [48]. DRhFe was developed by linking rhodamine spirolactam and dansylamide through an Fe^{3+} ionophore N^2−hydroxyethyldiethylenetriamine.

Free DRhFe showed inherent fluorescence of dansylamide at 483 nm. Upon reacting with Fe^{3+}, Fe^{3+} chelation could facilitate the transformation of rhodamine spirolactam into spiroring−open form, accompanied by the arising of a new absorption peak at 561 nm and fluorescence emission peak at 576 nm, corresponding to the formation of rhodamine B. At the same time, as the overlap of rhodamine's absorption band (500−600 nm) and dansylamide's emission band (440−560 nm), intramolecular FRET between dansylamide (FRET donor) and rhodamine (FRET acceptor) could result in emission shift from 483 to 576 nm. DRhFe is also sensitive and selective for Fe^{3+}, with limit of detection determined to be 0.13 μM. The addition of various metal ions, such as Fe^{2+}, Co^{2+}, Ni^{2+}, Cu^{2+}, did not produce notable response even at a 20 equiv concentration level. Notably, the response of DRhFe to Fe^{3+} is reversible. In the presence of transition−metal chelator N,N,N',N'−tetrakis(2−pyridylmethyl) ethylenediamine (TPEN), Fe^{3+} could be deprived from the DRhBFe/Fe complex to recover the fluorescence of DRhFe. Colocalization of DRhFe with commercially available dyes for organelle verified the subcellular distribution of this probe in endoplasmic reticulum and lysosome. Finally, DRhFe was applied to monitor labile Fe^{3+} fluctuations in cells undergoing ferroptosis. A pretreatment of HeLa cells with ferroptosis inducer erastin for 8 h resulted in a 2.1−fold fluorescence ratio increase relative to control, revealing the enhanced intracellular labile Fe^{3+} levels during ferroptosis.
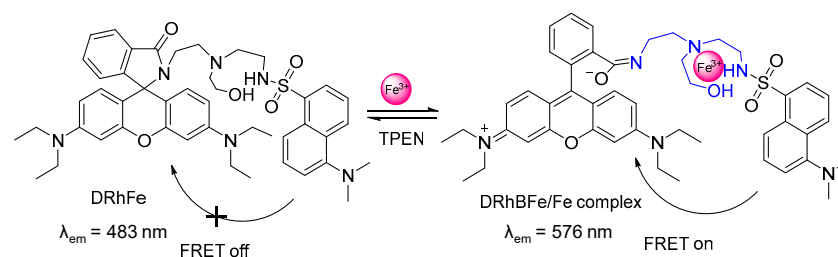

Figure 7. The reversible response mechanism of DRhFe to Fe^{3+} [48].

3. Fluorescence Probes for ROS

An important feature of ferroptosis is the aberrant accumulation of intracellular ROS, which then play critical roles in the production of lipid peroxides [30,31]. Besides the commercially available ROS fluorescence probes, such as H_2DCF−DA for the total ROS, selective ROS fluorescence probes for •OH, H_2O_2, hypochlorite (OCl^-) and peroxynitrite ($ONOO^-$) have been developed and applied in ferroptosis.

3.1. Probes for •OH

Usually, •OH reacts with other reactants via three type of reactions, electrophilic hydroxylation of aromatic compounds, hydrogen atom abstraction, or monoelectronic oxidation [49]. The design of •OH−selective probe also mainly depends on these reactions.

As one of the most reactive forms of ROS, •OH is capable of initiating lipid peroxidation because of its strong hydrogen abstraction ability [50]. Moreover, the primarily sources of •OH in biosystems are Fenton reaction and Haber–Weiss reaction [28,29], both of which are highly dependent on the participation of iron, similar to ferroptosis. Therefore, it is presumed that ferroptosis is featured by increased •OH level. However, in the previous studies, due to the lack of selectivity for •OH, the commonly used ROS probe H_2DCF−DA failed to reveal how the •OH levels vary during ferroptosis. Therefore, Li et al. [51] reported a selective •OH probe H−V (Figure 8), and applied it to reveal the •OH level changing behavior in ferroptosis for the first time. H−V was designed based on the unique aromatic hydroxylation ability of •OH, which is more selective for •OH than those based on oxidation reactions. The symmetric structure with two small π−conjugations of H−V gave rise to its short absorption and emission wavelengths. Upon reacting to •OH, the hydroxylation by •OH at 4−position of the middle benzene could form a phenol intermediate, which then undergoes deprotonation, electron rearrangement and π−conjugation extension to eventually form a near infrared (NIR) fluorescent product with emission at 652 nm. On the

other hand, the "molecular rotor" feature of H−V resulted in its viscosity−dependent fluorescence increase (see the detail mechanisms in Section 5.2 below), enables the detection of microenvironmental viscosity at 520 nm, which is separated from the •OH detection channel. H−V is selective for •OH and viscosity, unaffected by other ROS (e.g., OCl$^-$, ONOO$^-$, H$_2$O$_2$, O$_2$$^{•-}$ even at 10 equiv concentration level) and environmental factors (e.g., polarity and pH). With the fluorescence imaging of H−V, ferroptosis of HT−1080 cells treated with erastin or RSL3 was found to be accompanied by significant •OH generation, cytoplasmic viscosity increase, and accelerated lipid droplet formation. Notably, the generated •OH is probably the main cause of lipid peroxidation, which thus leads to the increase in cytoplasmic viscosity and the accelerated formation of lipid droplet. These features of ferroptosis were also seen in another ferroptosis−susceptible cell line, 786−O cells, suggesting they are not cell−line selective.
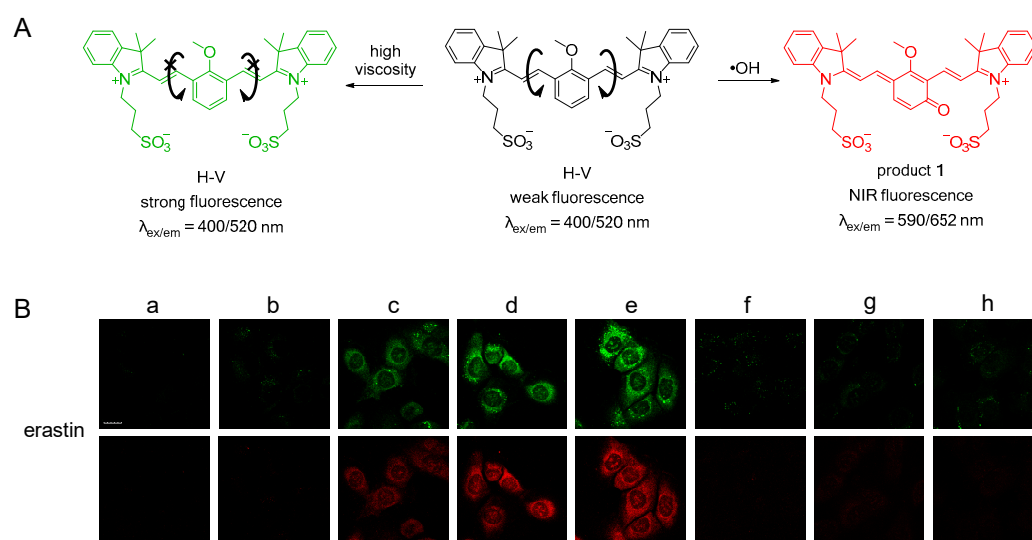

Figure 8. The •OH and viscosity dual−functional fluorescence probe H−V and its application in imaging of changes in •OH level and cytoplasmic viscosity during erastin−initiated ferroptosis of HT−1080 cells. (**A**) Response mechanism of H−V to •OH and viscosity. (**B**) Fluorescence images of HT−1080 cells under different conditions. (**a**) Cells only. (**b–e**) Cells pretreated with erastin for (**b**) 0 h, (**c**) 4 h, (**d**) 6 h, or (**e**) 8 h and then incubated with H−V for imaging. (**f–h**) Cells pretreated with erastin in the presence of ferroptosis inhibitor (**f**) DFO, (**g**) Fer−1, or (**h**) Lip−1 for 8 h and then incubated H−V for imaging. Green channel and red channel reflected the changes in cytoplasmic viscosity and •OH level, respectively. Reprinted/adapted with permission from Ref. [51]. Copyright 2019, American Chemical Society.

Due to the crucial and highly related roles of •OH and Cys in the development and redox regulation in ferroptosis, our group [52] developed a fluorescence probe Coum−HCy for the dual−functional detection of •OH and Cys (Figure 9). Coum−HCy is composed of a coumarin fluorophore and a commonly used recognition site hydrocyanine moiety for •OH [53,54]. When reacting with •OH, Coum−HCy gets hydrogen abstracted by •OH to form a larger π−conjugation and produce obvious spectra red shift to 650 nm, achieving a low−background NIR fluorescence detection of •OH to improve sensitivity. Sequentially, through a series of reactions such as nucleophilic substitution, structure rearrangement and Michael addition [55], the chloride atom and polymethine chain of the former product can react with Cys to produce fluorescence response at 453 nm. This unique π−conjugation extension and shortening of Coum−HCy enabled the sequential detection of •OH and Cys in two separated fluorescence channels without spectral interference. Coum−HCy is selective for •OH and Cys, unaffected from other common ROS (including O$_2$$^{•-}$, OCl$^-$, ONOO$^-$, ^{1}O$_2$, and H$_2O_2$) and biothiols (including GSH, Hcy and NAC). Coum−HCy was applied for the in situ monitoring of •OH and Cys level change during ferroptosis initiated

by erastin or RSL3, respectively. In consistent with the previous reports, ●OH was found to be significantly generated in both the erastin−initiated and RSL3−initiated ferroptosis process. On the other hand, during erastin−initiated ferroptosis, the intracellular Cys level obviously decreases due to the block of cystine (Cys precursor) uptake by erastin, whereas during the different initiating mechanism of ferroptosis by RSL3, the Cys level remains unaffected during RSL3−initiated ferroptosis. The dual−functional detection of ●OH and Cys by Coum−HCy through such a sequential response would streamline the detection processes and provide more accurate information about ●OH and Cys, and thus it is expected to be applied in more ferroptosis−related studies.
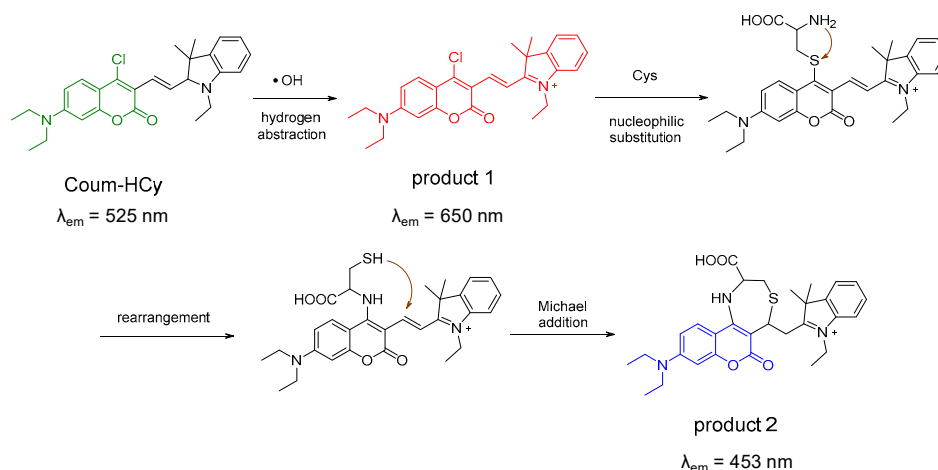

Figure 9. The sequential response mechanism of Coum−HCy to ●OH and Cys. Reprinted/adapted with permission from Ref. [52]. Copyright 2022, Elsevier.

3.2. Probes for H_2O_2

H_2O_2 is a relative stable and mild ROS. Boronate ester is one of the most commonly used recognition group for H_2O_2 [56,57]. In response to H_2O_2, aromatic boronate ester can be oxidized to its corresponding phenol product, which usually results in the fluorescence of the connected fluorophore increase or alteration. In recent years, several boronate ester−based probes have been developed and applied for imaging of H_2O_2 in ferroptosis. However, it should be noted that boronate ester is not very selective for H_2O_2. In some reported probes, boronate ester is also used as the recognition site for other ROS such as $ONOO^-$ and OCl^-, due to their faster oxidation rates than H_2O_2 [58–61].

In 2020, Li [62] developed a boronate ester−based probe HP for detection of H_2O_2 in ferroptosis (Figure 10A). HP was designed by connecting boronate ester and a dicyanoisophorone fluorophore, and showed obvious fluorescence increase in response to H_2O_2. It is sensitive and selective to H_2O_2, with a limit of detection to be 0.77 μM and no interference from some common bioactive species, for example, OCl^-, Cys, Fe^{2+}, Fe^{3+}, GSH and H_2S. HP has been used to image the change in intracellular H_2O_2 level regulated by the H_2O_2 inducer or activator, and visualize the significant H_2O_2 release in HepG2 cells incubated with ferroptosis inducer erastin for 12 h, revealing it as a feature of ferroptosis process.

Some organic fluorophores have a unique excited−state intramolecular proton−transfer (ESIPT) process, i.e., proton transfer from hydroxyl (−OH) or amino (−NH_2) to the close carbonyl group or nitrogen atom of heterocycle under photoexcitation, and possess many advantages, such as large Stokes shifts, environmental sensitivity and dual fluorescence emission [63,64]. Taking advantage of the ESIPT fluorescence turn−on mechanism, Zhou's group [65] reported a boronate ester−based probe BTFMB (Figure 10B). It is constructed by using an ESIPT fluorophore 2−(2′−hydroxyphenyl) benzothiazole. After reacting with H_2O_2, BTFMB displayed an obvious fluorescence increase at 542 nm with excitation at 380 nm (Stokes shift 162 nm). BTFMB was also applied for monitoring the H_2O_2

level increase during the erastin−induced ferroptosis process in HepG2 cells. However, $ONOO^-$ could produce comparable response with H_2O_2, which would disturb the detection of H_2O_2.
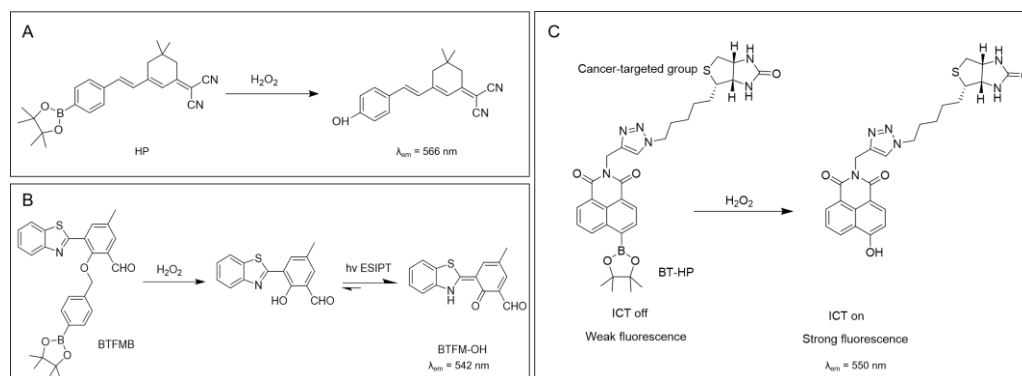

Figure 10. The response mechanism of (**A**) HP [62], (**B**) BTFMB [65] and (**C**) BT−HP [66] with H_2O_2.

Biotin is a widely used cancer cell−targeting group as the overexpression of biotin receptors in many types of cancer cells. By being modified with a biotin group, a tumor−targeting two−photon H_2O_2 probe BT−HP (Figure 10C) was developed by Kong's [66] group with 1,8−naphthalimide as fluorophore. BT−HP is selective for H_2O_2 over other ROS including OCl^- and $ONOO^-$. BT−HP was capable of depth−penetration imaging of H_2O_2 in cancer cells and tumor tissues by two−photon microscope. BT−HP was further applied to detect H_2O_2 in cancer cells during the ferroptosis process.

3.3. Probe for OCl^-

OCl^- is the product of H_2O_2 and chloride ions through the enzymatic reaction by myeloperoxidase (MPO). It plays important roles in many diseases, such as epilepsy, and thus might be a promising biomarker for the early diagnosis of epilepsy and a potential therapeutic target for epilepsy. Qian's group [67] developed a two−photon fluorescence probe HCP for OCl^- (Figure 11), and applied it for monitor the OCl^- level change in the kainic acid−induced cell ferroptosis and epileptic model of mice. HCP was designed by a Schiff base functionalized 6−(dimethylamino)quinolone−2−carbaldehyde with a diaminomaleonitrile. HCP itself displayed a weak yellow fluorescence, which was resulted from the diminished push–pull electron effect of quinolone fluorophore by the conjugated electron−acceptor diaminomaleonitrile group. By contrast, in the presence of OCl^-, the chlorination of quinolone fluorophore to form HCP−Cl would lead to alteration of the intermolecular electronic effect and achieving an enhanced fluorescence response at 495 nm. HCP was capable of fast (within 5 s), selective (over other ROS including •OH, $O_2^{\bullet-}$, H_2O_2 and $ONOO^-$) and sensitive (limit of detection to be 104 nM) detection of OCl^-. HCP was used to directly visualize the endogenous OCl^- overproduction both in living cells and in vivo, such as in human neuroblastoma SH−SY5Y cells treated with lipopolysaccharide or MPO + H_2O_2 + Cl^-, kainic acid−induced SH−SY5Y cell ferroptosis and epileptic model of mice. In addition, taking advantage of the fluorescence imaging of HCP, the authors have constructed a high−throughput screening approach to rapidly screen the potential antiepileptic agents from a mass of natural products, and identified that the flavonoid compound apigenin can relieve the MPO−mediated oxidative stress and inhibit the ferroptosis of neuronal cells and is a potential antiepileptic agent.
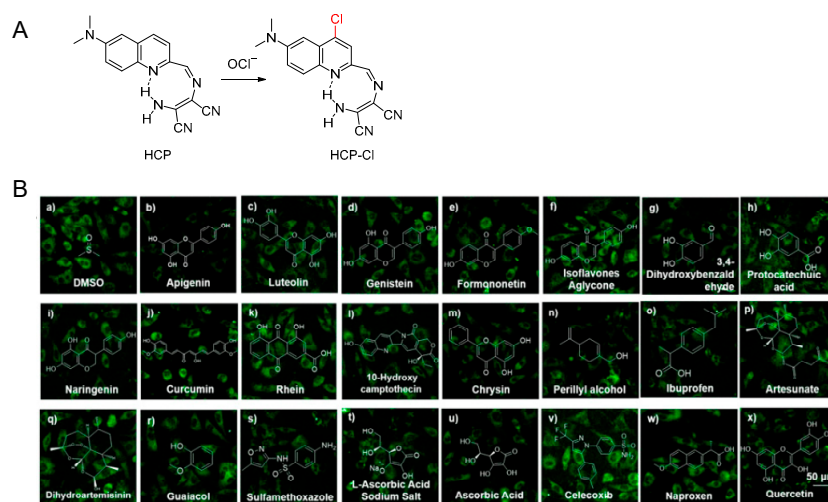
Figure 11. (**A**) Response mechanism of HCP to OCl$^-$. (**B**) High$-$throughput screening of potential antiepileptic agents from natural products by HCP. Reprinted/adapted with permission from Ref. [67]. Copyright 2020, National Academy of Sciences.

3.4. Probe for ONOO$^-$

ONOO$^-$ is the product of O$_2^{\bullet-}$ and nitric oxide (NO) and one of the most cytotoxic ROS. The overproduction of ONOO$^-$ is suggested to be one of the predominant executioner of regulated cell death. Tang's group [68] develop a two$-$photon fluorescence probe NATP (Figure 12) for ONOO$^-$ and applied it to study the connections between ONOO$^-$ overproduction and ferroptosis of neuronal cells. NATP was designed by functionalizing naphthalimide fluorophore with a oxindole as recognition site for ONOO$^-$. After treatment with ONOO$^-$, the decyclization of oxindole could obtain a primary aniline product, accompanied by obvious fluorescence increase. NATP was then employed to image the neuronal PC12 cells, revealing up$-$regulated ONOO$^-$ level in PC12 cells upon Aβ peptide treatment. Further studies by incubating PC12 cells with Aβ peptide in the presence of ferroptosis inhibitor Fer$-$1 or deferiprone, or by examining the expression level of GPX4 through Western blot analysis revealed Aβ peptide can induce cell death via the ferroptotic pathway. Additionally, NATP was used to establish a high$-$throughput fluorescence$-$based screening method to screen the potential neuroprotective natural products. Most importantly, NATP has good blood–brain barrier penetrability and is capable of in situ visualizing the cerebral ONOO overproduction in Alzheimer's disease mice.
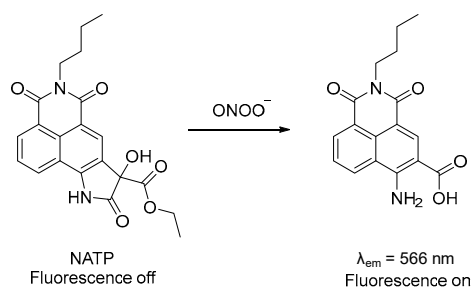

Figure 12. Response mechanism of NATP to ONOO$^-$ [68].

4. Fluorescence Probes for Biothiols

Biothiols, including Cys and GSH, are the major reductive regulators of ferroptosis process. The initiation of ferroptosis involves in dysfunction of intracellular biothiols [11], such as inhibition of the system x_c^- on cell membrane to block the import of cystine and deplete biothiols, or inhibition GPX4 activity to prevent the scavenging of lipid peroxides by GSH. Therefore, the selective and in situ detection of Cys and GSH by fluorescence

probes are of great significance to the studies of ferroptosis. In addition, fluorescence probes for the downstream products of Cys and GSH, such as hydrogen sulfide (H_2S) and hydrogen polysulfide (H_2S_n), have also been reported to applied in ferroptosis.

4.1. Probe for Cys

Qian's group [69] developed a fluorescence probe CP2 for monitoring the Cys level change in living cells and in vivo mediated by system x_c^- (Figure 13). CP2 was constructed by modifying a dicyanoisophorone fluorophore with an acrylate group, which acted as recognizing site for cysteine and could effectively quench the fluorescence of dicyanoisophorone fluorophore. CP2 can specifically recognize Cys and give a fluorescence turn−on response at 568 nm, unaffected by other common biothiols including GSH, Hcy and H_2S. With the dynamic tracking of Cys level in living cells by CP2, the decrease in intracellular Cys level upon blocking system x_c^- activity to induce ferroptotic cell death by erastin was revealed. Notably, with the imaging of CP2, cancer cells were observed to have relatively higher level of endogenous Cys, which could be also effectively regulated by the inhibition of system x_c^-. Moreover, the block of system x_c^- to induce ferroptosis by erastin could be synergized with the cysteine biosynthesis inhibitor to improve anti-cancer efficacy (especially against lung cancer cells) and overcome the cisplatin resistance of cisplatin−resistant lung cancer A549R cells, which might bring a new approach for treating drug−resistant carcinoma. Furthermore, in vivo imaging of Cys by CP2 in zebrafishes upon erastin−induced ferroptosis verified its potential capability for live−animal Cys visualization.
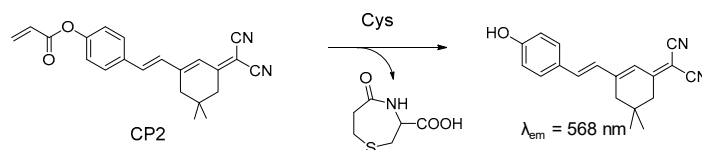

Figure 13. Response mechanism of CP2 to Cys [69].

4.2. Probe for GSH

Real−time dynamic monitoring of GSH concentration changes remains many obstacles, such as reaction reversibility, kinetics of the sensing reaction as well as the high concentration of intracellular GSH. Making use of the inherent reversibility of Michael addition reaction, in 2017, Jiang et al. [70] reported a reversible reaction−based fluorescence probe, RealThiol (RT), that can quantitatively monitor the real−time GSH dynamics in living cells (Figure 14A). RT was designed based on its Michael addition reaction with GSH, which is inherently reversible with an appropriate dissociation constant K_d (mM range, comparable to the physiological GSH concentration). Furthermore, the cyano group at the α position of the Michael acceptor is favorable to accelerate the response reaction, which enables the real−time monitoring of GSH level change. In addition, a four−membered azetidine ring was induced to improve the spectroscopic properties of the probe; two carboxylic acid groups were induced to improve the aqueous solubility and avoid the binding of probe with hydrophobic cellular constituents. RT and its GSH adduct RT−GSH showed different fluorescence at 487 and 562 nm with excitation at 405 and 488 nm, respectively, which allowed ratiometric imaging of GSH quantification independent of the probe concentration. In reaction kinetics studies, RT showed fast kinetics in both forward and reverse reactions, with a second−order reaction rate constant 7.5 M^{-1} s^{-1} between RT and GSH, and a first−order dissociation reaction rate constant 20.3 $\times$ 10^{-3} s^{-1} for RT−GSH, which is thus capable of real−time dynamic monitoring of GSH level increase and decrease in a minute−level time resolution (Figure 14B). With RT, GSH level changes during ferroptosis had been visualized. The results showed that despite significant morphology changes, GSH levels do not immediately decrease after erastin treatment over 3 min time span (Figure 14C).
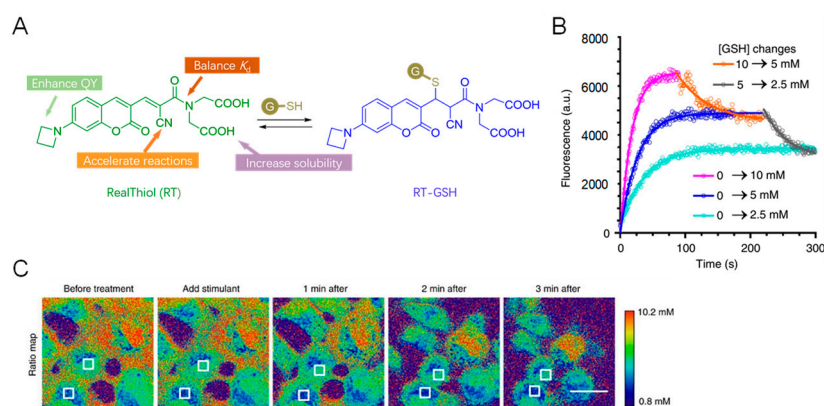
Figure 14. (**A**) The reversible response mechanism of RT to GSH. (**B**) Dynamic and reversible monitoring of GSH level changes by RT. (**C**) Ratiometric imaging of dynamic GSH changes during ferroptosis induced by erastin in HT−1080 cells. Reprinted/adapted with permission from Ref. [70]. Copyright 2017, The Authors.

4.3. Probe for H_2S

Probes for reducing substances (such as H_2S) usually consume reducing substances, instigating a redox imbalance, which further aggravates the progression of ferroptosis. Therefore, Hu's group [71] developed an H_2S−triggered and H_2S−releasing NIR fluorescence probe (HL−H_2S) for the high−fidelity in situ imaging of ferroptosis (Figure 15). When HL−H_2S responded to H_2S, the reduction of azido group to amine could trigger 1,6−elimination to release the NIR fluorescent HL−NH_2, as well as carbonyl sulfide (O=C=S), which was then catalyzed by carbonic anhydrase to form H_2S. Thus, the detection of H_2S in ferroptosis would avoid the consumption of H_2S. Additionally, the rotatable vinyl bond of the released fluorophore HL−NH_2 enabled its fluorescence increase response to viscosity, which contributed the accurate detection of the ferroptosis process because cell viscosity increases during ferroptosis. Furthermore, using erastin as an inducer for ferroptosis, the observed trends for ferroptosis biomarkers, such as Fe^{2+}, MDA, and GSH, indicated that the introduction of the HL−H_2S did not exacerbate ferroptosis. HL−H_2S was finally applied to image H_2S decrease in ferroptosis during oxygen glucose deprivation/re−oxygenation in PC12 cells and middle cerebral artery occlusion model in mice.
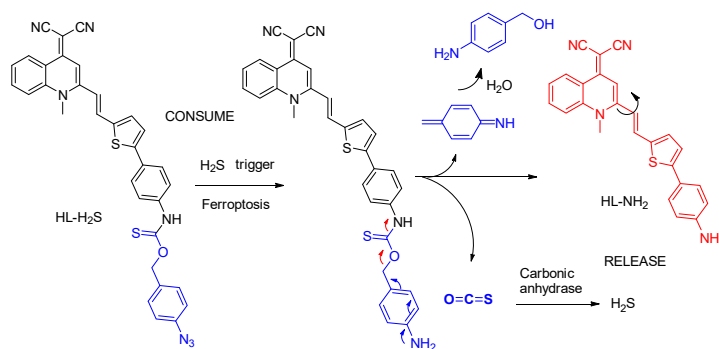

Figure 15. The H_2S−triggered NIR fluorescence response and H_2S release mechanism of HL−H_2S [71].

4.4. Probe for H_2S_n

H_2S_n (n > 1), the oxidized product of H_2S and ROS, is an important member of biothiols, and plays crucial roles in regulating the activities of ion channels, transcription factors, protein kinases, and tumor suppressors. To develop a detection method that is capable of in situ monitoring of H_2S_n to study its molecular mechanisms in the process

of ferroptosis, Qian's group [72] reported a two−photon NIR fluorescence probe PSP for H_2S_n (Figure 16). PSP was designed by utilized an dicyanoisophorone−derived naphthalene as fluorophore and the 2−fluoro−5−nitrobenzoate as the responsive group for H_2S_n. The probe itself exhibited almost no fluorescence because of quenching effect of the 2−fluoro−5−nitrobenzoate group. Upon addition of H_2S_n, the 2−fluoro−5−nitrobenzoate group was selectively deprotected to release the fluorophore with NIR emission at 640 nm and good two−photon cross−section. Furthermore, with the in situ and dynamic imaging of PSP during ferroptotic cell death of HeLa cells induced by erastin, the up−regulated H_2S_n level was revealed as a feature of ferroptosis, which might be promoted by the overproduction of ROS during ferroptosis.
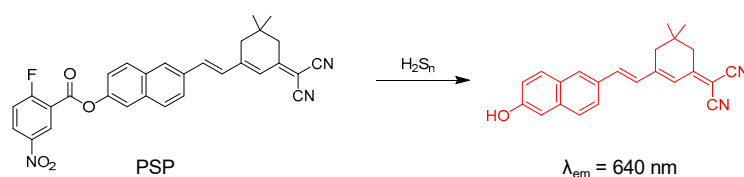

Figure 16. The two−photon NIR fluorescence response of PSP and H_2S_n [72].

5. Fluorescence Probes for Cell Microenvironmental Factors

Cell microenvironmental factors, such as viscosity and polarity, play vital roles in many cell physiological and pathological processes. For example, viscosity affects the diffusion of biological active species and transportation of signals [73]; polarity can reflect the interaction activity between enzymes and proteins [74]. Probes for tracking cell microenvironmental viscosity and polarity during ferroptosis have also attracted many research interests in recent years.

5.1. Probe for Polarity

In general, the fluorescence of a fluorophore with a donor (D)−π−acceptor (A) structure is usually sensitive to its ambient environment polarity. With the increase in environmental polarity, fluorescence of the fluorophore will become weak and shift to longer emission wavelength due to the dissipation of the excited state energy resulting from the enhanced dipole–dipole interaction between the fluorophores and solvent molecules [75].

Liu's group [76] reported a lipid droplets (LDs) and nucleus dual−targeted ratiometric fluorescence probe CQPP for monitoring polarity changes in the cellular microenvironment. As shown in Figure 17A, CQPP has a typical polarity−susceptible D−π−A molecular structure. It was designed by the integration of coumarin unit (donor) and the cationic quinolinium (acceptor) with further extended 1−(pyridin−4−yl)piperazine group, to mimic Nile Red (a commercial LDs dye) and Hoechst 33,342 (a commercial nucleus dye). CQPP presented a red shift of fluorescence emission with the increase in the environment polarity (Figure 17B). Profiting from the LDs/nucleus dual−targetable and ratiometric responsive properties, CQPP was applied to monitor polarity changes in LDs using nucleus imaging as a reference during ferroptosis. As shown in Figure 17C, in the control group, compared to the cytoplasm, LDs displayed significantly lower polarities, with a polarity increasing gradient from its core (red color) to the surface (blue color). However, in the erastin−induced ferroptosis group, the fluorescence in green channel in LDs is gradually decreased, and slightly increased in red channel of the cytoplasm, indicating the increase in LDs polarity during ferroptosis. Similarly, LDs polarity increase was also observed in RSL3−induced ferroptosis as well as gradual homogeneity of polarity between LDs and cytoplasm (Figure 17D). Besides, CQPP was also capable of monitoring LDs polarity increase in ferroptosis by fluorescence lifetime imaging.
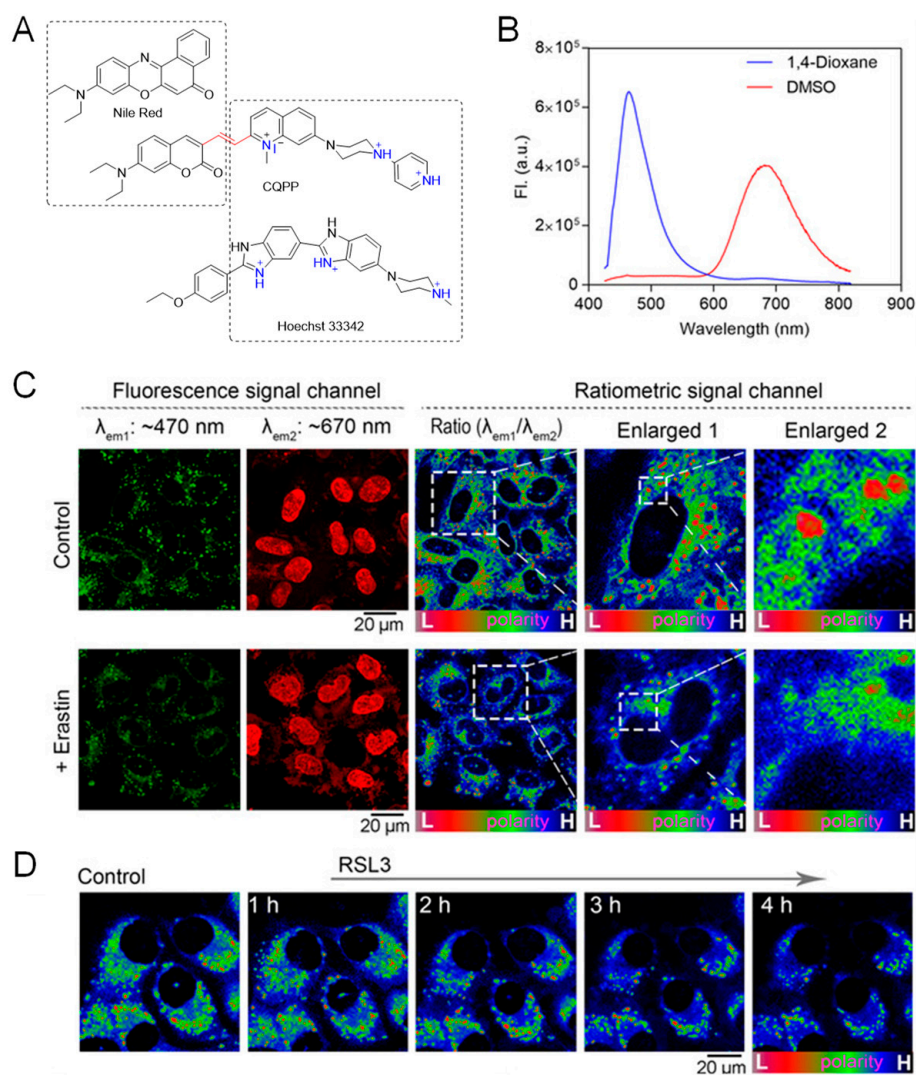
Figure 17. Polarity responsive probe CQPP and its application in ferroptosis. (**A**) Molecule design of CQPP. (**B**) Emission spectra of CQPP in 1,4−dioxane (low polarity) and DMSO (high polarity). (**C**) Imaging of polarity changes in erastin−induced ferroptosis. (**D**) Imaging of polarity changes in RSL3−induced ferroptosis. Reprinted/adapted with permission from Ref. [76]. Copyright 2021, Wiley−VCH GmbH.

　　　Ye's group [77] developed a LDs targeting dual−functional fluorescence probe TPA−SO$_2$ for monitoring polarity change and SO$_2$ level during ferroptosis (Figure 18). In TPA−SO$_2$, a triphenylamine group was introduced as LDs targeting group. At the same time, a C=C double bond served as recognition site for SO$_2$. As a result, TPA−SO$_2$ presented strong red fluorescence at 610 nm in low polarity medium, accompanied by fluorescence decrease and red shift with the increase in polarity. On the other hand, in the presence of SO$_2$, as the Michael addition reaction between TPA−SO$_2$ and SO$_2$, TPA−SO$_2$ showed obvious fluorescence increase at 437 nm, which enabled the independent detection of polarity and SO$_2$ in two separate channels. TPA−SO$_2$ was applied for imaging of polarity change and SO$_2$ level in HeLa cells during ferroptosis, which revealed increased concentration of endogenous SO$_2$ and polarity.
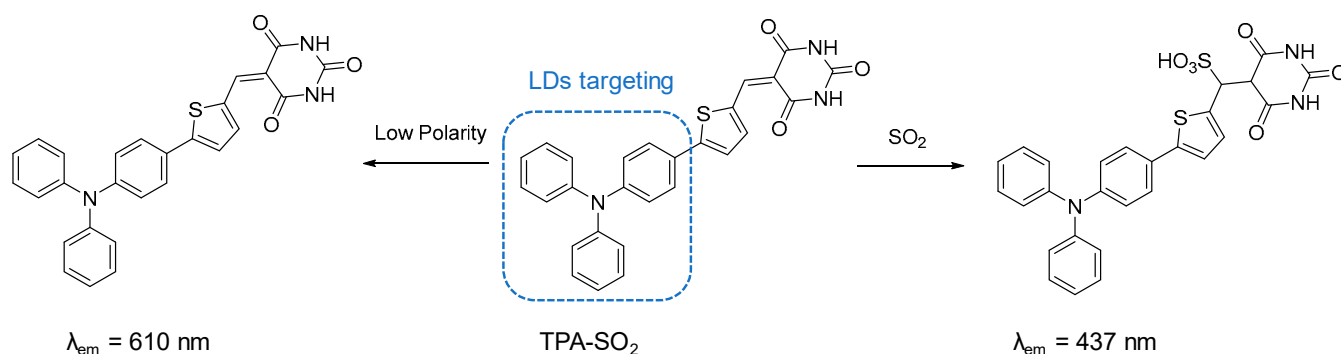
Figure 18. Response mechanism of TPA−SO$_2$ to polarity and SO$_2$ [77].

5.2. Probes for Viscosity

In general, the fluorophores sensitive to environmental viscosity share similar molecular rotor structure, in which an electron donor and an electron acceptor are connected by a rotatable bond (e.g., vinyl bond) to form a D−π−A structure [78,79]. Under low viscosity environment, the free rotation of the rotatable bond can efficiently weaken the fluorescence or shorten the fluorescence lifetime of the fluorophore through a nonradiative deactivation process called twisted intramolecular charge transfer (TICT) [80]. However, with the increase in environmental viscosity, the rotation is inhibited, which can thus result in enhanced fluorescence signals or longer fluorescence lifetime.

Lipid droplets (LDs), is the main storage organelle for lipids, including neutral lipids, unsaturated lipids and lipid peroxides with different viscosities. Due to the significant lipid peroxidation during ferroptosis, the targeting detection of viscosity changes in LDs is not only usable for monitoring ferroptosis process, but also important for deep study of the biological roles of LDs during ferroptosis. Therefore, Lin's group [81] reported a LDs targetable probe BDHT for monitoring LDs viscosity change in ferroptosis (Figure 19). BDHT has a typical molecular rotor and D−π−A structure, and thus it is sensitive for viscosity changes. UV−vis absorption and fluorescence spectra tests were firstly conducted to study the response of BDHT to viscosity. In the low viscous methanol solution, BDHT showed an absorption peak at 502 nm, which gradually shifted to 529 nm with solvent viscosity increase by the addition of viscous glycerol to methanol, accompanied by decreased absorbance. On the other hand, BDHT showed a 21−fold increase in emission intensity at 723 nm under excitation at 620 nm, with fluorescence quantum yields increasing from 0.12% (in methanol) to 10.9% (in glycerol). BDHT is selective for viscosity change, unaffected by other environmental factors, such as pH and polarity. BDHT was finally used for specific detection of LDs viscosity changes in ferroptosis. HeLa cells, 4T1 cells, A545 cells, or HepG2 cells treated with ferroptosis inducer erastin or RSL3 all presented time−dependent fluorescence increase in BDHT, indicating the gradually increase in LDs viscosity during ferroptosis in different type of cell lines.
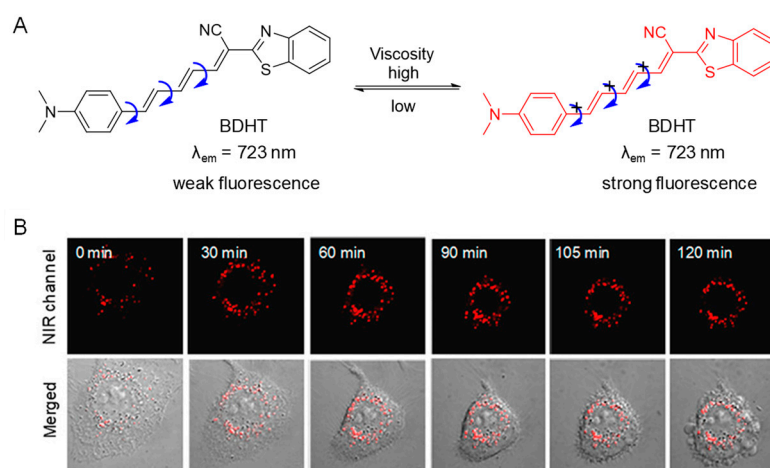
Figure 19. BDHT and its application in ferroptosis. (**A**) NIR fluorescence increase mechanism of BDHT with the increase in viscosity. (**B**) Imaging of LDs viscosity increase in erastin−induced ferroptosis of HeLa cells. Reprinted/adapted with permission from Ref. [81]. Copyright 2021, American Chemical Society.

More recently, Lin's group [82] developed an endoplasmic reticulum targeting dual −functional fluorescence probe DSPI−3 for monitoring viscosity and pH change (Figure 20). In DSPI−3, the rotatable cyanine dye acts as viscosity response moiety, naphthalimide dye serves as pH response moiety. With the increase in environmental viscosity, the restriction of C=C bond rotation could result in fluorescence increase at 620 nm. On the other hand, with the decrease in pH value, protonation of the piperazine group connected with naphthalimide dye would cut down the PET effect from piperazine to naphthalimide, achieving a fluorescence increase at 528 nm. With the fluorescence imaging of DSPI−3, acidification and viscosity increase in endoplasmic reticulum during ferroptosis process induced by erastin were found. In addition, when cells co−cultured with dithiothreitol and erastin, endoplasmic reticulum pH value considerably decreased at the early stage, but slightly increased in the later stage; meanwhile, endoplasmic reticulum viscosity enhanced slowly at the early stage, and declined in the later stage, demonstrating that dithiothreitol can accelerate ferroptosis via inducing endoplasmic reticulum stress.
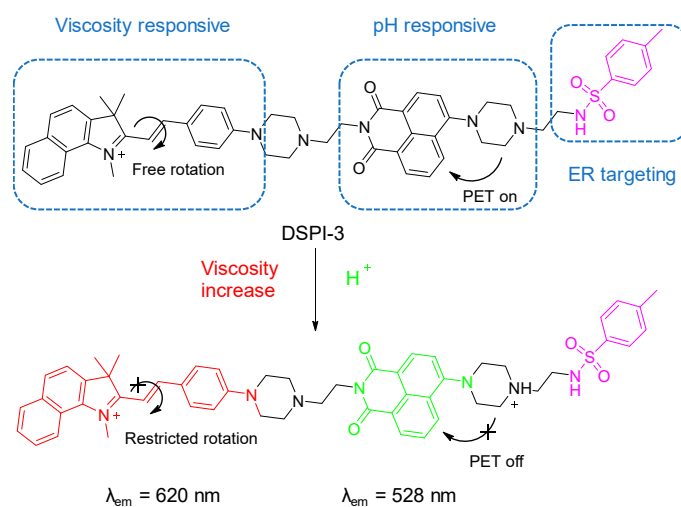

Figure 20. Response mechanism of DSPI−3 to viscosity and pH [82].

NAD(P)H, the reduced nicotinamide adenine dinucleotide and its phosphorylated form, are important coenzymes, participate in many cellular metabolic processes in living cells. Recently, it is reported NAD(P)H participate in several antioxidant processes to

modulate ferroptosis. Therefore, tracking of intracellular NAD(P)H level during ferroptosis is important. Wei et al. [83] reported a mitochondrial targeting dual−functional probe 3Q−2 (Figure 21). It was capable of detecting mitochondrial viscosity and NAD(P)H level in two different fluorescence channels. Firstly, due to its molecular rotor and positive charged structure, 3Q−2 was able to target mitochondria and showed fluorescence enhancement at 550 nm upon viscosity increase. In addition, the quinolinium of 3Q−2 is a commonly used recognition group for NAD(P)H. In the presence of NAD(P)H, the reduction of quinolinium to the electron−rich enamine moiety could produce a product with D−π−A structure, and the strong intermolecular charge transfer (ICT) effect from enamine to the electron−withdrawing malononitrile group could result in a NIR turn−on emission at 670 nm with large Stokes shift, enabling the independent detection of NAD(P)H in a separated signal channel from viscosity. With the imaging of 3Q−2, the authors found that the levels of intracellular NAD(P)H and mitochondrial viscosity in HT−1080 cells were significantly increased by treatment with erastin or RSL3, but with a weaker trend in the case of RSL3 compared to cells induced by erastin.
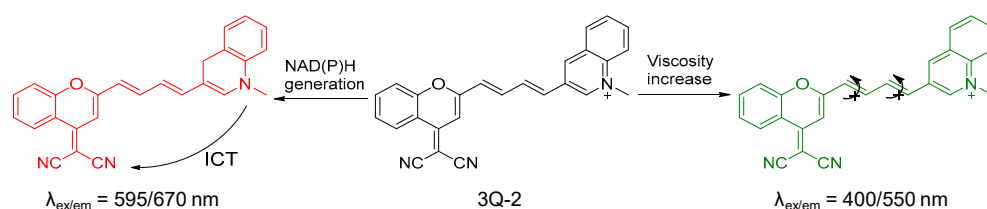

Figure 21. Response mechanism of 3Q−2 to viscosity and NAD(P)H [83].

Yin et al. [84] reported another mitochondria−targeted probe MN−V for detection of mitochondrial viscosity changes in ferroptosis process (Figure 22). In MN−V, benzoindolium acted as both electron acceptor and mitochondria−targeting group as its positive charge. MN−V had two absorption maximum at 687 nm and 730 nm, respectively. In the non−viscous PBS, its fluorescence emission peak can hardly be detected. However, with the increase in viscosity (glycerol ratio increase in the glycerol–PBS mixtures) from 1.2 cP to 980 cP, the emission peak at 795 nm of the probe increased 37 times. MN−V had good mitochondria−targeting ability (Pearson's coefficient 0.93 with commercially available mitochondrial dye). MN−V was finally used for imaging of the mitochondrial viscosity increase in HeLa cells during ferroptosis.
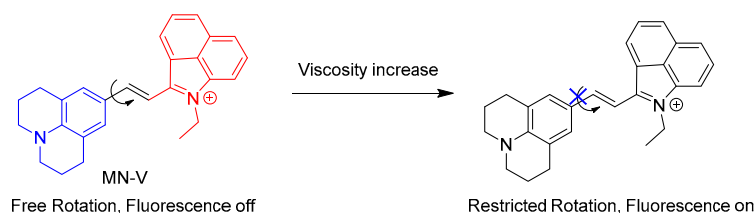

Figure 22. NIR fluorescence increase mechanism of MN−V with the increase in viscosity [84].

In addition, by modified a BODIPY fluorophore with an endoplasmic reticulum targetable sulfonamide group via click reaction, Xiao's group [85] reported a viscosity sensitive probe L−Vis−1 for tracking endoplasmic reticulum viscosity changes in endoplasmic reticulum (Figure 23). L−Vis−1 showed 26−fold fluorescence enhancement at 515 nm with viscosity increase from 1.8 cP to 950 cP (glycerol ratio of the glycerol–methanol mixtures from 10% to 99%). Moreover, the increased viscosity also resulted in longer fluorescence lifetime of L−Vis−1, enabling quantitative detection of microviscosity via fluorescence lifetime model. With fluorescence imaging and fluorescence lifetime imaging of L−Vis−1, apparent local viscosity increases in endoplasmic reticulum were observed during the ferroptosis process induced by erastin and artesunate for the first time.
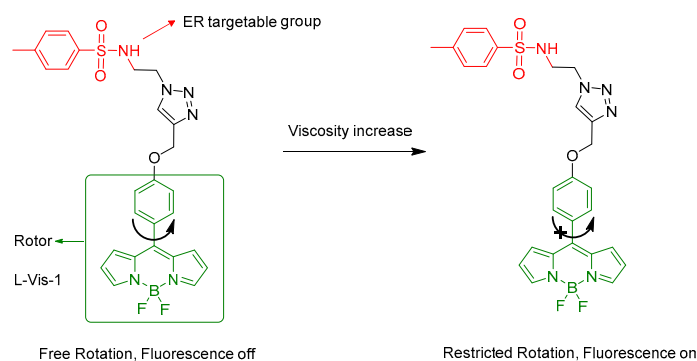
Figure 23. Design of L−Vis−1 and its fluorescence response mechanism to viscosity [85].

6. Conclusions

In this review, we have summarized and discussed a series of fluorescence probes for the selective analysis of iron, ROS, biothiols as well as intracellular microenvironmental factors in ferroptosis. Taking advantage of these probes, many interesting and important changes of bioactive species levels and intracellular microenvironmental factors during ferroptosis have been revealed, such as an increase in ●OH, labile heme level and LDs polarity, and a decrease in H_2S level, which provide critical evidence for understanding ferroptosis. However, there still remain some problems or difficulties in the current developments and applications of fluorescence probes for monitoring the ferroptosis process. Firstly, the complicacy of intracellular physiological species and ferroptosis regulation mechanisms makes it is difficult to illustrate the exact roles of the analyte in the development of ferroptosis and related diseases with a single fluorescence probe. Secondly, the commonly used commercially available probe C11−BODIPY$^{581/591}$ for lipid peroxides can only monitor the total amount of lipid peroxides, and it lacks selectivity for a certain lipid peroxide. Therefore, selective probes for lipid peroxides are in urgent need of development. Some possible study trends are listed below. 1. Development of a probe for independent analysis of multi−analyte to simplify the detection procedures and provide more accurate information to indicate the possible mutual correlation of these analytes. 2. Comprehensive comparison of the differences in bioactive species level change between ferroptosis and other regulated cell death. 3. Applications in ferroptosis at animal level with specific disease models. It is believed that more important features and pathogenic roles of ferroptosis will be found with the development of new tailored fluorescence probes. We hope that this review will help the ongoing development and application of fluorescence probes in ferroptosis.

Institutional Review Board Statement: Not applicable.

Informed Consent Statement: Not applicable.

Data Availability Statement: Not applicable.

Conflicts of Interest: The authors declare no conflict of interest.

References

1. Dixon, S.J.; Lemberg, K.M.; Lamprecht, M.R.; Skouta, R.; Zaitsev, E.M.; Gleason, C.E.; Patel, D.N.; Bauer, A.J.; Cantley, A.M.; Yang, W.S.; et al. Ferroptosis: An Iron−Dependent Form of Nonapoptotic Cell Death. *Cell* **2012**, *149*, 1060–1072. [CrossRef] [PubMed]
2. Dixon, S.J.; Stockwell, B.R. The Hallmarks of Ferroptosis. *Annu. Rev. Cancer Biol.* **2019**, *3*, 35–54. [CrossRef]
3. Jiang, X.; Stockwell, B.R.; Conrad, M. Ferroptosis: Mechanisms, Biology and Role in Disease. *Nat. Rev. Mol. Cell Biol.* **2021**, *22*, 266–282. [CrossRef] [PubMed]
4. Wang, F.; Graham, E.T.; Naowarojna, N.; Shi, Z.; Wang, Y.; Xie, G.; Zhou, L.; Salmon, W.; Jia, J.M.; Wang, X.; et al. PALP: A Rapid Imaging Technique for Stratifying Ferroptosis Sensitivity in Normal and Tumor Tissues in Situ. *Cell Chem. Biol.* **2022**, *29*, 157–170. [CrossRef] [PubMed]
5. Distéfano, A.M.; Martin, M.V.; Córdoba, J.P.; Bellido, A.M.; D'Ippólito, S.; Colman, S.L.; Soto, D.; Roldán, J.A.; Bartoli, C.G.; Zabaleta, E.J.; et al. Heat Stress Induces Ferroptosis−like Cell Death in Plants. *J. Cell Biol.* **2017**, *216*, 463–476. [CrossRef] [PubMed]
6. Liang, C.; Zhang, X.; Yang, M.; Dong, X. Recent Progress in Ferroptosis Inducers for Cancer Therapy. *Adv. Mater.* **2019**, *31*, 1904197. [CrossRef] [PubMed]
7. Hadian, K.; Stockwell, B.R. A Roadmap to Creating Ferroptosis−Based Medicines. *Nat. Chem. Biol.* **2021**, *17*, 1113–1116. [CrossRef] [PubMed]
8. Ma, W.; Gao, Y.; Ouyang, Z.; Fan, Y.; Yu, H.; Zhan, M.; Wang, H.; Shi, X.; Shen, M. Apoptosis−Enhanced Ferroptosis Therapy of Pancreatic Carcinoma through PAMAM Dendrimer−Iron(III) Complex−Based Plasmid Delivery. *Sci. China Chem.* **2022**, *65*, 778–788. [CrossRef]
9. Zhang, N.; Shu, G.; Qiao, E.; Xu, X.; Shen, L.; Lu, C.; Chen, W.; Fang, S.; Yang, Y.; Song, J.; et al. DNA−Functionalized Liposomes In Vivo Fusion for NIR−II/MRI Guided Pretargeted Ferroptosis Therapy of Metastatic Breast Cancer. *ACS Appl. Mater. Interfaces* **2022**, *14*, 20603–20615. [CrossRef] [PubMed]
10. Xie, L.; Li, J.; Wang, G.; Sang, W.; Xu, M.; Li, W.; Yan, J.; Li, B.; Zhang, Z.; Zhao, Q.; et al. Phototheranostic Metal−Phenolic Networks with Antiexosomal PD−L1 Enhanced Ferroptosis for Synergistic Immunotherapy. *J. Am. Chem. Soc.* **2022**, *144*, 787–797. [CrossRef] [PubMed]
11. Stockwell, B.R.; Friedmann Angeli, J.P.; Bayir, H.; Bush, A.I.; Conrad, M.; Dixon, S.J.; Fulda, S.; Gascón, S.; Hatzios, S.K.; Kagan, V.E.; et al. Ferroptosis: A Regulated Cell Death Nexus Linking Metabolism, Redox Biology, and Disease. *Cell* **2017**, *171*, 273–285. [CrossRef]
12. Yang, W.S.; Stockwell, B.R. Ferroptosis: Death by Lipid Peroxidation. *Trends Cell Biol.* **2016**, *26*, 165–176. [CrossRef] [PubMed]
13. Byun, J.K.; Lee, S.; Kang, G.W.; Lee, Y.R.; Park, S.Y.; Song, I.S.; Yun, J.W.; Lee, J.; Choi, Y.K.; Park, K.G. Macropinocytosis Is an Alternative Pathway of Cysteine Acquisition and Mitigates Sorafenib−Induced Ferroptosis in Hepatocellular Carcinoma. *J. Exp. Clin. Cancer Res.* **2022**, *41*, 98. [CrossRef] [PubMed]
14. Zhou, Z.; Liang, H.; Yang, R.; Yang, Y.; Dong, J.; Di, Y.; Sun, M. Glutathione Depletion-Induced Activation of Dimersomes for Potentiating the Ferroptosis and Immunotherapy of "Cold" Tumor. *Angew. Chem. Int. Ed.* **2022**, *61*, e202202843.
15. Yang, W.S.; SriRamaratnam, R.; Welsch, M.E.; Shimada, K.; Skouta, R.; Viswanathan, V.S.; Cheah, J.H.; Clemons, P.A.; Shamji, A.F.; Clish, C.B.; et al. Regulation of Ferroptotic Cancer Cell Death by GPX4. *Cell* **2014**, *156*, 317–331. [CrossRef] [PubMed]
16. Tian, X.; Murfin, L.C.; Wu, L.; Lewis, S.E.; James, T.D. Fluorescent Small Organic Probes for Biosensing. *Chem. Sci.* **2021**, *12*, 3406–3426. [CrossRef]
17. Zhou, J.; Ma, H. Design Principles of Spectroscopic Probes for Biological Applications. *Chem. Sci.* **2016**, *7*, 6309–6315. [CrossRef] [PubMed]
18. Li, X.; Gao, X.; Shi, W.; Ma, H. Design Strategies for Water−Soluble Small Molecular Chromogenic and Fluorogenic Probes. *Chem. Rev.* **2014**, *114*, 590–659. [CrossRef] [PubMed]
19. Chen, X.; Wang, F.; Hyun, J.Y.; Wei, T.; Qiang, J.; Ren, X.; Shin, I.; Yoon, J. Recent Progress in the Development of Fluorescent, Luminescent and Colorimetric Probes for Detection of Reactive Oxygen and Nitrogen Species. *Chem. Soc. Rev.* **2016**, *45*, 2976–3016. [CrossRef]
20. Han, H.H.; Tian, H.; Zang, Y.; Sedgwick, A.C.; Li, J.; Sessler, J.L.; He, X.P.; James, T.D. Small−Molecule Fluorescence−Based Probes for Interrogating Major Organ Diseases. *Chem. Soc. Rev.* **2021**, *50*, 9391–9429. [CrossRef] [PubMed]
21. Zeng, Z.; Liew, S.S.; Wei, X.; Pu, K. Hemicyanine−Based Near−Infrared Activatable Probes for Imaging and Diagnosis of Diseases. *Angew. Chem. Int. Ed.* **2021**, *60*, 26454–26475. [CrossRef]
22. Zhang, J.; Chai, X.; He, X.P.; Kim, H.J.; Yoon, J.; Tian, H. Fluorogenic Probes for Disease−Relevant Enzymes. *Chem. Soc. Rev.* **2019**, *48*, 683–722. [CrossRef] [PubMed]
23. Zhou, Y.; Wang, X.; Zhang, W.; Tang, B.; Li, P. Recent Advances in Small Molecule Fluorescent Probes for Simultaneous Imaging of Two Bioactive Molecules in Live Cells and in Vivo. *Front. Chem. Sci. Eng.* **2022**, *16*, 4–33. [CrossRef]
24. Wu, X.; Shi, W.; Li, X.; Ma, H. Recognition Moieties of Small Molecular Fluorescent Probes for Bioimaging of Enzymes. *Acc. Chem. Res.* **2019**, *52*, 1892–1904. [CrossRef] [PubMed]
25. Zhao, Y.; Shi, W.; Li, X.; Ma, H. Recent Advances in Fluorescent Probes for Lipid Droplets. *Chem. Commun.* **2022**, *58*, 1495–1509. [CrossRef]
26. Gao, M.; Yi, J.; Zhu, J.; Minikes, A.M.; Monian, P.; Thompson, C.B.; Jiang, X. Role of Mitochondria in Ferroptosis. *Mol. Cell* **2019**, *73*, 354–363. [CrossRef] [PubMed]

27. Torii, S.; Shintoku, R.; Kubota, C.; Yaegashi, M.; Torii, R.; Sasaki, M.; Suzuki, T.; Mori, M.; Yoshimoto, Y.; Takeuchi, T.; et al. An Essential Role for Functional Lysosomes in Ferroptosis of Cancer Cells. *Biochem. J.* **2016**, *473*, 769–777. [CrossRef] [PubMed]

28. Marques, O.; da Silva, B.M.; Porto, G.; Lopes, C. Iron Homeostasis in Breast Cancer. *Cancer Lett.* **2014**, *347*, 1–14. [CrossRef] [PubMed]

29. Valko, M.; Rhodes, C.J.; Moncol, J.; Izakovic, M.; Mazur, M. Free Radicals, Metals and Antioxidants in Oxidative Stress−Induced Cancer. *Chem. Biol. Interact.* **2006**, *160*, 1–40. [CrossRef]

30. Foret, M.K.; Lincoln, R.; Do Carmo, S.; Cuello, A.C.; Cosa, G. Connecting the "Dots": From Free Radical Lipid Autoxidation to Cell Pathology and Disease. *Chem. Rev.* **2020**, *120*, 12757–12787. [CrossRef]

31. Latunde−Dada, G.O. Ferroptosis: Role of Lipid Peroxidation, Iron and Ferritinophagy. *Biochim. Biophys. Acta Gen. Subj.* **2017**, *1861*, 1893–1900. [CrossRef] [PubMed]

32. Kagan, V.E.; Mao, G.; Qu, F.; Angeli, J.P.F.; Doll, S.; Croix, C.S.; Dar, H.H.; Liu, B.; Tyurin, V.A.; Ritov, V.B.; et al. Oxidized Arachidonic and Adrenic PEs Navigate Cells to Ferroptosis. *Nat. Chem. Biol.* **2017**, *13*, 81–90. [CrossRef] [PubMed]

33. Varnes, A.W.; Dodson, R.B.; Wehry, E.L. Interactions of Transition−Metal Ions with Photoexcited States of Flavines. Fluorescence Quenching Studies. *J. Am. Chem. Soc.* **1972**, *94*, 946–950. [CrossRef] [PubMed]

34. Kemlo, J.A.; Shepherd, T.M. Quenching of Excited Singlet States by Metal Ions. *Chem. Phys. Lett.* **1977**, *47*, 158–162. [CrossRef]

35. Irving, H.; Williams, R.J.P. 637. The Stability of Transition−Metal Complexes. *J. Chem. Soc.* **1953**, 3192–3210. [CrossRef]

36. Aron, A.T.; Loehr, M.O.; Bogena, J.; Chang, C.J. An Endoperoxide Reactivity−Based FRET Probe for Ratiometric Fluorescence Imaging of Labile Iron Pools in Living Cells. *J. Am. Chem. Soc.* **2016**, *138*, 14338–14346. [CrossRef]

37. Hirayama, T.; Okuda, K.; Nagasawa, H. A Highly Selective Turn−on Fluorescent Probe for Iron(II) to Visualize Labile Iron in Living Cells. *Chem. Sci.* **2013**, *4*, 1250–1256. [CrossRef]

38. Aron, A.T.; Reeves, A.G.; Chang, C.J. Activity−Based Sensing Fluorescent Probes for Iron in Biological Systems. *Curr. Opin. Chem. Biol.* **2018**, *43*, 113–118. [CrossRef]

39. Hirayama, T.; Kadota, S.; Niwa, M.; Nagasawa, H. A Mitochondria−Targeted Fluorescent Probe for Selective Detection of Mitochondrial Labile Fe(II). *Metallomics* **2018**, *10*, 794–801. [CrossRef]

40. Niwa, M.; Hirayama, T.; Okuda, K.; Nagasawa, H. A New Class of High−Contrast Fe(II) Selective Fluorescent Probes Based on Spirocyclized Scaffolds for Visualization of Intracellular Labile Iron Delivered by Transferrin. *Org. Biomol. Chem.* **2014**, *12*, 6590–6597. [CrossRef]

41. Hirayama, T.; Tsuboi, H.; Niwa, M.; Miki, A.; Kadota, S.; Ikeshita, Y.; Okuda, K.; Nagasawa, H. A Universal Fluorogenic Switch for Fe(II) Ion Based on N−Oxide Chemistry Permits the Visualization of Intracellular Redox Equilibrium Shift towards Labile Iron in Hypoxic Tumor Cells. *Chem. Sci.* **2017**, *8*, 4858–4866. [CrossRef] [PubMed]

42. Hirayama, T.; Miki, A.; Nagasawa, H. Organelle−Specific Analysis of Labile Fe(II) during Ferroptosis by Using a Cocktail of Various Colour Organelle−Targeted Fluorescent Probes. *Metallomics* **2019**, *11*, 111–117. [CrossRef]

43. Kawai, K.; Hirayama, T.; Imai, H.; Murakami, T.; Inden, M.; Hozumi, I.; Nagasawa, H. Molecular Imaging of Labile Heme in Living Cells Using a Small Molecule Fluorescent Probe. *J. Am. Chem. Soc.* **2022**, *144*, 3793–3803. [CrossRef]

44. Groves, J.T.; Watanabe, Y. Reactive Iron Porphyrin Derivatives Related to the Catalytic Cycles of Cytochrome P−450 and Peroxidase. Studies of the Mechanism of Oxygen Activation. *J. Am. Chem. Soc.* **1988**, *110*, 8443–8452. [CrossRef]

45. Xing, W.; Xu, H.; Ma, H.; Abedi, S.A.A.; Wang, S.; Zhang, X.; Liu, X.; Xu, H.; Wang, W.; Lou, K. A PET−Based Fluorescent Probe for Monitoring Labile Fe(II) Pools in Macrophage Activations and Ferroptosis. *Chem. Commun.* **2022**, *58*, 2979–2982. [CrossRef] [PubMed]

46. Gui, R.; Jin, H.; Bu, X.; Fu, Y.; Wang, Z.; Liu, Q. Recent Advances in Dual−Emission Ratiometric Fluorescence Probes for Chemo/Biosensing and Bioimaging of Biomarkers. *Coord. Chem. Rev.* **2019**, *383*, 82–103. [CrossRef]

47. Zuo, Y.; Yang, T.; Wang, X.; Zhang, Y.; Tian, M.; Gou, Z.; Lin, W. Visualizing the Cell Ferroptosis via a Novel Polysiloxane−Based Fluorescent Schiff Base. *Sens. Actuators Chem.* **2019**, *298*, 126843. [CrossRef]

48. Gao, J.; He, Y.; Chen, Y.; Song, D.; Zhang, Y.; Qi, F.; Guo, Z.; He, W. Reversible FRET Fluorescent Probe for Ratiometric Tracking of Endogenous Fe3+ in Ferroptosis. *Inorg. Chem.* **2020**, *59*, 10920–10927. [CrossRef] [PubMed]

49. Gligorovski, S.; Strekowski, R.; Barbati, S.; Vione, D. Environmental Implications of Hydroxyl Radicals (●OH). *Chem. Rev.* **2015**, *115*, 13051–13092. [CrossRef]

50. Yin, H.; Xu, L.; Porter, N.A. Free Radical Lipid Peroxidation: Mechanisms and Analysis. *Chem. Rev.* **2011**, *111*, 5944–5972. [CrossRef]

51. Li, H.; Shi, W.; Li, X.; Hu, Y.; Fang, Y.; Ma, H. Ferroptosis Accompanied by ●OH Generation and Cytoplasmic Viscosity Increase Revealed via Dual−Functional Fluorescence Probe. *J. Am. Chem. Soc.* **2019**, *141*, 18301–18307. [CrossRef]

52. Chen, Y.; Hu, Z.; Yang, M.; Gao, J.; Luo, J.; Li, H.; Yuan, Z. Monitoring the Different Changing Behaviors of ●OH and Cysteine in Two Ferroptosis Pathways by a Dual−Functional Fluorescence Probe. *Sens. Actuators Chem.* **2022**, *362*, 131742. [CrossRef]

53. Wang, J.Y.; Liu, Z.R.; Ren, M.; Kong, X.; Liu, K.; Deng, B.; Lin, W. A Fast−Responsive Turn on Fluorescent Probe for Detecting Endogenous Hydroxyl Radicals Based on a Hybrid Carbazole−Cyanine Platform. *Sens. Actuators Chem.* **2016**, *236*, 60–66. [CrossRef]

54. Yuan, L.; Lin, W.; Song, J. Ratiometric Fluorescent Detection of Intracellular Hydroxyl Radicals Based on a Hybrid Coumarin−Cyanine Platform. *Chem. Commun.* **2010**, *46*, 7930–7932. [CrossRef] [PubMed]

55. He, X.; Wu, X.; Shi, W.; Ma, H. N−Acetylcysteine and Cysteine in Their Ability to Replenish Intracellular Cysteine by a Specific Fluorescent Probe. *Chem. Commun.* **2016**, *52*, 9410–9413. [CrossRef]

56. Li, H.; Ma, H. New Progress in Spectroscopic Probes for Reactive Oxygen Species. *J. Anal. Test.* **2018**, *2*, 2–19. [CrossRef]

57. Jiao, X.; Li, Y.; Niu, J.; Xie, X.; Wang, X.; Tang, B. Small−Molecule Fluorescent Probes for Imaging and Detection of Reactive Oxygen, Nitrogen, and Sulfur Species in Biological Systems. *Anal. Chem.* **2018**, *90*, 533–555. [CrossRef]

58. Xu, Q.; Lee, K.A.; Lee, S.; Lee, K.M.; Lee, W.J.; Yoon, J. A Highly Specific Fluorescent Probe for Hypochlorous Acid and Its Application in Imaging Microbe−Induced Hocl Production. *J. Am. Chem. Soc.* **2013**, *135*, 9944–9949. [CrossRef]

59. Kim, J.; Park, J.; Lee, H.; Choi, Y.; Kim, Y. A Boronate−Based Fluorescent Probe for the Selective Detection of Cellular Peroxynitrite. *Chem. Commun.* **2014**, *50*, 9353–9356. [CrossRef] [PubMed]

60. Zhou, J.; Li, Y.; Shen, J.; Li, Q.; Wang, R.; Xu, Y.; Qian, X. A Ratiometric Fluorescent Probe for Fast and Sensitive Detection of Peroxynitrite: A Boronate Ester as the Receptor to Initiate a Cascade Reaction. *RSC Adv.* **2014**, *4*, 51589–51592. [CrossRef]

61. Li, H.; Liu, Y.; Li, X.; Li, X.; Ma, H. Design, Synthesis and Application of a Dual−Functional Fluorescent Probe for Reactive Oxygen Species and Viscosity. *Spectrochim. Acta Part Mol. Biomol. Spectrosc.* **2021**, *246*, 119059. [CrossRef] [PubMed]

62. Li, Z. Imaging of Hydrogen Peroxide (H2O2) during the Ferroptosis Process in Living Cancer Cells with a Practical Fluorescence Probe. *Talanta* **2020**, *212*, 120804. [CrossRef]

63. Sedgwick, A.C.; Wu, L.; Han, H.H.; Bull, S.D.; He, X.P.; James, T.D.; Sessler, J.L.; Tang, B.Z.; Tian, H.; Yoon, J. Excited−State Intramolecular Proton−Transfer (ESIPT) Based Fluorescence Sensors and Imaging Agents. *Chem. Soc. Rev.* **2018**, *47*, 8842–8880. [CrossRef] [PubMed]

64. Mishra, V.R.; Ghanavatkar, C.W.; Sekar, N. Towards NIR−Active Hydroxybenzazole (HBX)−Based ESIPT Motifs: A Recent Research Trend. *ChemistrySelect* **2020**, *5*, 2103–2113. [CrossRef]

65. Zhang, H.C.; Tian, D.H.; Zheng, Y.L.; Dai, F.; Zhou, B. Designing an ESIPT−Based Fluorescent Probe for Imaging of Hydrogen Peroxide during the Ferroptosis Process. *Spectrochim. Acta Part Mol. Biomol. Spectrosc.* **2021**, *248*, 119264. [CrossRef]

66. Ren, M.; Dong, D.; Xu, Q.; Yin, J.; Wang, S.; Kong, F. A Biotin−Guided Two−Photon Fluorescent Probe for Detection of Hydrogen Peroxide in Cancer Cells Ferroptosis Process. *Talanta* **2021**, *234*, 122684. [CrossRef] [PubMed]

67. Shao, C.; Yuan, J.; Liu, Y.; Qin, Y.; Wang, X.; Gu, J.; Chen, G.; Zhang, B.; Liu, H.K.; Zhao, J.; et al. Epileptic Brain Fluorescent Imaging Reveals Apigenin Can Relieve the Myeloperoxidase−Mediated Oxidative Stress and Inhibit Ferroptosis. *Proc. Natl. Acad. Sci. USA* **2020**, *117*, 10155–10164. [CrossRef]

68. Xie, X.; Liu, Y.; Liu, G.; Zhao, Y.; Liu, J.; Li, Y.; Zhang, J.; Jiao, X.; Wang, X.; Tang, B. Two−Photon Fluorescence Imaging of the Cerebral Peroxynitrite Stress in Alzheimer's Disease. *Chem. Commun.* **2022**, *58*, 6300–6303. [CrossRef] [PubMed]

69. Li, Z.; Li, Y.; Yang, Y.; Gong, Z.; Zhu, H.; Qian, Y. In Vivo Tracking Cystine/Glutamate Antiporter−Mediated Cysteine/Cystine Pool under Ferroptosis. *Anal. Chim. Acta* **2020**, *1125*, 66–75. [CrossRef]

70. Jiang, X.; Chen, J.; Bajić, A.; Zhang, C.; Song, X.; Carroll, S.L.; Cai, Z.L.; Tang, M.; Xue, M.; Cheng, N.; et al. Quantitative Real−Time Imaging of Glutathione. *Nat. Commun.* **2017**, *8*, 16087. [CrossRef] [PubMed]

71. Liang, T.; Qiang, T.; Ren, L.; Cheng, F.; Wang, B.; Li, M.; Hu, W.; James, T.D. Near−Infrared Fluorescent Probe for Hydrogen Sulfide: High−Fidelity Ferroptosis Evaluation in Vivo during Stroke. *Chem. Sci.* **2022**, *13*, 2992–3001. [CrossRef]

72. Di, X.; Ge, C.; Liu, Y.; Shao, C.; Zhu, H.L.; Liu, H.K.; Qian, Y. Monitoring Hydrogen Polysulfide during Ferroptosis with a Two−Photon Fluorescent Probe. *Talanta* **2021**, *232*, 122467. [CrossRef] [PubMed]

73. Kao, H.P.; Abney, J.R.; Verkman, A.S. Determinants of the Translational Mobility of a Small Solute in Cell Cytoplasm. *J. Cell Biol.* **1993**, *120*, 175–184. [CrossRef]

74. Olzmann, J.A.; Carvalho, P. Dynamics and Functions of Lipid Droplets. *Nat. Rev. Mol. Cell Biol.* **2019**, *20*, 137–155. [CrossRef]

75. Wang, S.; Ren, W.X.; Hou, J.T.; Won, M.; An, J.; Chen, X.; Shu, J.; Kim, J.S. Fluorescence Imaging of Pathophysiological Microenvironments. *Chem. Soc. Rev.* **2021**, *50*, 8887–8902. [CrossRef] [PubMed]

76. Wang, K.N.; Liu, L.Y.; Mao, D.; Xu, S.; Tan, C.P.; Cao, Q.; Mao, Z.W.; Liu, B. A Polarity−Sensitive Ratiometric Fluorescence Probe for Monitoring Changes in Lipid Droplets and Nucleus during Ferroptosis. *Angew. Chem. Int. Ed.* **2021**, *60*, 15095–15100. [CrossRef] [PubMed]

77. Xie, P.; Liu, J.; Yang, X.; Zhu, W.; Ye, Y. A Bifunctional Fluorescent Probe for Imaging Lipid Droplets Polarity/SO2 during Ferroptosis. *Sens. Actuators Chem.* **2022**, *365*, 131937. [CrossRef]

78. Kuimova, M.K. Mapping Viscosity in Cells Using Molecular Rotors. *Phys. Chem. Chem. Phys.* **2012**, *14*, 12671–12686. [CrossRef] [PubMed]

79. Lee, S.C.; Heo, J.; Woo, H.C.; Lee, J.A.; Seo, Y.H.; Lee, C.L.; Kim, S.; Kwon, O.P. Fluorescent Molecular Rotors for Viscosity Sensors. *Chem. Eur. J.* **2018**, *24*, 13706–13718. [CrossRef]

80. Abdel−Mottaleb, M.S.A.; Loutfy, R.O.; Lapouyade, R. Non−Radiative Deactivation Channels of Molecular Rotors. *J. Photochem. Photobiol. A Chem.* **1989**, *48*, 87–93. [CrossRef]

81. Dong, B.; Song, W.; Lu, Y.; Sun, Y.; Lin, W. Revealing the Viscosity Changes in Lipid Droplets during Ferroptosis by the Real−Time and in Situ Near−Infrared Imaging. *ACS Sens.* **2021**, *6*, 22–26. [CrossRef] [PubMed]

82. Song, W.; Zhang, W.; Yue, L.; Lin, W. Revealing the Effects of Endoplasmic Reticulum Stress on Ferroptosis by Two−Channel Real−Time Imaging of PH and Viscosity. *Anal. Chem.* **2022**, *94*, 6557–6565. [CrossRef] [PubMed]

83. Wei, H.; Yu, Y.; Wu, G.; Wang, Y.; Duan, S.; Han, J.; Cheng, W.; Li, C.; Tian, X.; Zhang, X. Dual−Responsive Fluorescent Probe for Imaging NAD(P)H and Mitochondrial Viscosity and Its Application in Cancer Cell Ferroptosis. *Sens. Actuators Chem.* **2022**, *350*, 130862. [CrossRef]

84. Yin, J.; Xu, Q.; Mo, X.; Dai, L.; Ren, M.; Wang, S.; Kong, F. Construction of a Novel Mitochondria−Targeted near−Infrared (NIR) Probe for Detection of Viscosity Changes in Cancer Cells Ferroptosis Process. *Dyes Pigments* **2022**, *200*, 110184. [CrossRef]

85. Liu, C.; Zhou, L.; Xie, L.; Zheng, Y.; Man, H.; Xiao, Y. Forthrightly Monitoring Ferroptosis Induced by Endoplasmic Reticulum Stresses through Fluorescence Lifetime Imaging of Microviscosity Increases with a Specific Rotor. *Chin. Chem. Lett.* **2021**, *33*, 2537–2540. [CrossRef]